

Boundary Element Analysis of Crack Propagation in Laser Scribing of Glass

Keisuke Yahata^{*}, Etsuji Ohmura^{*}, Seiji Shimizu^{**} and Masanao Murakami^{**}

^{*}Management of Industry and Technology, Osaka University, 2-1 Yamadaoka, Suita, Osaka 565-0871, Japan

E-mail: kyahata@mitsuboshi-dia.co.jp

^{**}Mitsuboshi Diamond Industrial Co., LTD., 32-12 Koroen, Settu, Osaka 566-0034, Japan

Laser scribing generates a shallow median crack on a glass surface as a pre-processing for division without physical contact. It utilizes thermal stress caused by heating with the laser beam and by cooling with the water jet. In laser scribing, different crack propagation phenomena are observed between the areas near and far from the glass edge. In this research, we examined experimentally how the crack propagates from the glass edge to the glass center. The crack propagation mechanism was considered through a crack propagation analysis where FEM and BEM are combined. The obtained conclusions are as follows: The initial crack propagates to become a through crack due to the tensile stress generated inside the glass during the period when the glass edge is heated. In the subsequent cooling period, large tensile stress is generated in the vicinity of the glass surface. The crack propagates quasi-steadily only in this region to become a surface crack of constant depth. The depth of the shallow crack can be estimated by the crack propagation analysis by setting a suitable threshold of the stress intensity factor.

DOI:10.2961/jlmn.2013.01.0020

Keywords: glass, CO₂ laser, thermal stress, scribing, FEM, BEM, three-dimensional analysis

1. Introduction

In recent years, the use of flat panel displays, laptop computers, and cell phones has grown, and the demands of liquid crystal displays (LCD) and plasma display panels (PDP) used in these products have grown as well. In the manufacturing of LCD or PDP, the glass cutting process is an indispensable step.

Glass is mainly divided by the scribe and break method. A mechanical process with a cutter wheel is widely applied in the scribing. However, due to the generation of microcracks on the scribed edge, the edge strength is decreased [1]. Due to the demands of high bending strength, especially in portable products, fewer microcracks should be generated.

Laser scribing is one of the non-contact scribing methods which causes no microcracks [2]. Figure 1 shows a schematic of the processing mechanism [3]. In this method an initial crack is first formed on the glass surface at the processing start point which is located at the glass edge. The glass surface is then heated by scanning the CO₂ laser beam. At the same time, the water jet is applied behind the laser beam and scanned at the same velocity, to quench the surface. The glass surface is heated by the laser beam and the heat diffuses to the interior. As a result, a high temperature region occurs in the vicinity of the surface, the region having a certain depth based on the diffusion of the laser energy. The water jet cools down the surface immediately after the laser beam irradiation. While the surface is cooled down, the interior still has a high temperature. Due to the sharp temperature gradient in the thickness direction, a compressive stress is generated inside the glass, and a tensile stress is generated in the vicinity of the surface. The tensile stress causes the initial crack to propagate, and a

shallow median crack is produced on the surface along the laser beam scanning line. It has been reported that the strength of the scribed edge is increased by applying this laser scribing [4].

Generally, the crack formed by the laser scribing propagates from the glass edge and has two distinct regions, a transitional crack near the glass edge and a shallow crack on the glass surface whose depth is constant far from the glass edge. That is to say, a crack of constant depth is created after the transitional crack propagation phenomenon. In conventional research, the crack propagation phenomena at the glass center have been considered experimentally and analytically. Yamamoto et al. [3] have explained the processing mechanism by comparing experimental and analytical results. And Yahata et al. [5] have reported that the crack depth at the glass center can be estimated by a two-dimensional crack propagation analysis.

However, we have not found papers which report the crack propagation mechanism in the region close to glass edges. Because the crack propagates across the substrate with the transitional phenomenon, it is important to understand the crack propagation mechanism not only at the

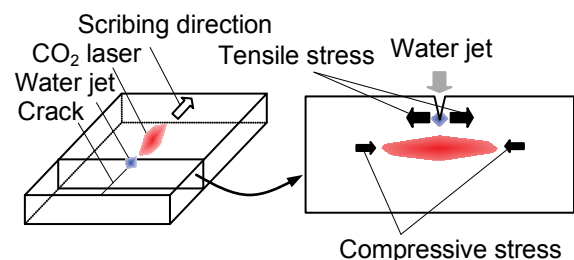


Fig. 1 Principle of laser scribing

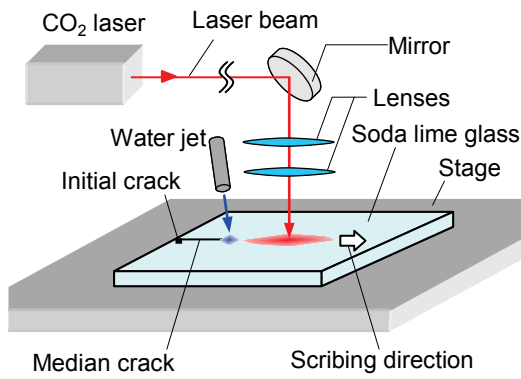


Fig. 2 Schematic of experimental setup

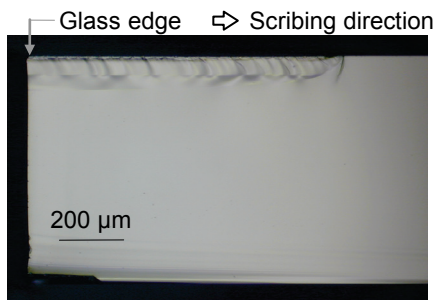


Fig. 3 Microscopic image of initial crack

glass center but also near glass edges. In this research, we investigated experimentally the crack propagation from the glass edge to the glass center. Then in order to clarify the mechanism of the crack propagation phenomena observed in the experiment, a three-dimensional crack propagation analysis was conducted.

In propagating the crack in the analysis, the stress intensity factor was calculated with a cracked model based on the thermal stress field obtained with an uncracked model. Regarding the thermal stress analysis with an uncracked model, the finite element method (FEM) was used as the conventional research [6]. On the other hand, to model the crack shape precisely in a three-dimensional analysis, many elements are generally necessary. Therefore, in the practical use, methods which reduce the analysis time are desired. In stress concentration problems, it has been reported that precise solutions can be obtained with fewer elements by the boundary element method (BEM) compared with FEM [7]. Therefore, in this research, we used BEM for the calculation of the stress intensity factor.

2. Laser scribing experiment

2.1 Experimental methodology

Laser scribing was conducted on soda-lime glass with a thickness of 700 μm in order to investigate how the crack propagates. The length of glass edge in the scribing direction was 230 mm. Figure 2 shows the schematic of the experimental setup. Because the experimental method is almost the same as that in our past report [5], the details are omitted here. An initial crack was first created mechanically at the processing start point, and then the laser beam and a water jet were scanned along the processing line. Figure 3 shows a microscopic image of the initial crack. It

Table 1 Processing conditions in experiment

v	Scribing velocity	40 - 400 mm/s
P	Laser power	50 - 90 W
$2\xi_h$	Minor axis of heating area	1.2 mm
$2\eta_h$	Major axis of heating area	26.0 mm
d	Cooling point distance	15.0 mm
$2\xi_c$	Minor axis of cooling area	2.0 mm
$2\eta_c$	Major axis of cooling area	3.0 mm

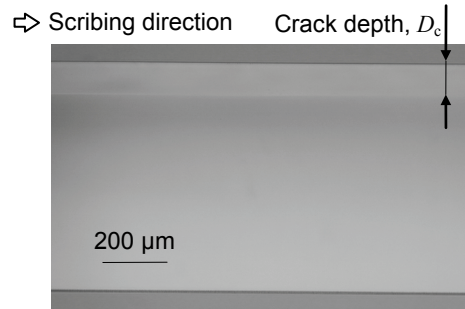


Fig. 4 Microscopic image of cutting plane at center of scribing line

was observed after dividing the substrate along the initial crack before the laser beam and the water jet were scanned. The upper surface in Fig. 3 is the surface along which the laser beam was irradiated during the processing. The initial crack depth at the glass edge and the length were approximately 100 μm and 1 mm respectively. Table 1 shows the experimental conditions. The cooling condition and the shape of the laser beam were set to be constant. The experiment was conducted under a variety of laser powers, P , and scanning velocities, v . After the processing, the substrate was divided along the crack and the crack propagation process was investigated by observing the cutting surface.

2.2 Experimental results

Under constant P , a crack is not formed at high scanning velocities, while thermal damages are generated at low scanning velocities [8]. The damaging conditions are unpractical due to the low edge strength. Therefore, we investigated the crack propagation process in cases where a median crack was formed without thermal damages.

Figure 4 shows a microscopic image of a cutting surface along a crack in the area distant from glass edges. The upper surface is the laser beam irradiated plane. The boundary line seen in the cutting surface shows the location of the crack front. As we have already reported [5], a crack of constant depth was formed at the glass center. Figure 5 shows the mean crack depth, D_c , under a variety of P and v , in which D_c was measured five times and the mean value was determined for each processing condition. As shown, D_c increased as P was increased and v was decreased.

In this research, we also investigated the crack propagation process near the processing start point. Figure 6 shows a microscopic image of the cutting surface near the initial crack. The upper surface is the laser beam irradiated plane. As shown, at point A, the crack front reached the rear surface of the substrate. On the other hand, in the region to the

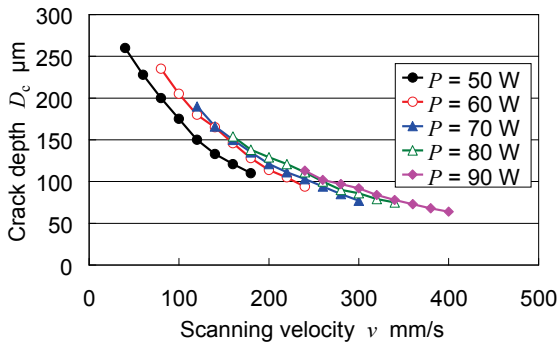


Fig. 5 Measured crack depth under a variety of P and v at center of scribing line

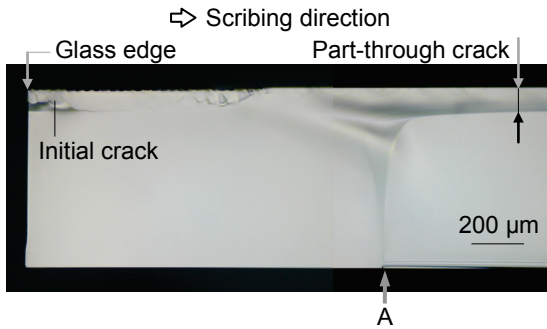


Fig. 6 Microscopic image of cutting plane near processing start

right of point A, a crack of constant depth was observed similarly to Fig. 4. From this result it is found that the initial crack created on the upper surface became a through crack which propagated to point A, and then transitioned into a surface crack of constant depth at point A. In all specimens we observed, this similar crack propagation process was observed.

3. Method of crack propagation analysis

3.1 Combination of FEM and BEM

In this research, we conduct three-dimensional crack propagation analyses based on the stress intensity factor, K , during the processing. As shown in Fig. 7 schematically, K is calculated based on the superposition principle. K should be obtained under a certain thermal stress distribution caused by a certain temperature distribution (Fig. 7 (a)). To obtain K , the thermal stress distribution in an uncracked model is first obtained (Fig. 7 (b)). Subsequently, the force distribution acting on crack surfaces is calculated and K is obtained (Fig. 7 (c)). A problem shown in Fig. 7 (b) is solved by FEM and that shown in Fig. 7 (c) is solved by BEM. Because a three-dimensional BEM analysis is conducted with two-dimensional elements, a crack shape is correctly modeled with fewer elements. We used the following commercially available software: ANSYS for FEM analyses and BEASY for BEM analyses.

3.2 Finite element analysis

Because the methodology of a finite element analysis is almost the same as that reported by Yamamoto et al. [6], the detail is omitted here. Figure 8 shows the mesh geometry. Each axis was set as follows. x : perpendicular direction to the scribing direction, y : scribing direction, z : thickness

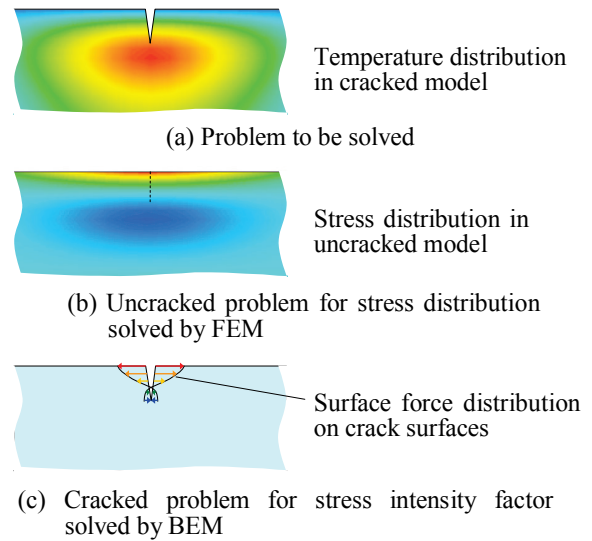


Fig. 7 Calculation method for stress intensity factor based on superposition principle

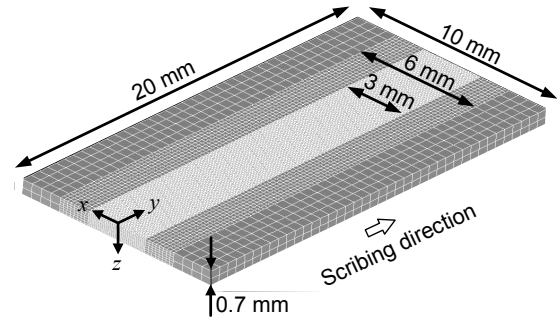


Fig. 8 Mesh geometry for FEM analysis

direction. The model size was $10\text{ mm} \times 20\text{ mm} \times 700\text{ }\mu\text{m}$. The origin and positive direction of each axis are also shown in Fig. 8. The processing location was set as $x = 0$ which means the center of the line of 10 mm length, and small elements are placed around the plane of $x = 0$. The minimum-sized element is a cuboid-shaped one sized $50\text{ }\mu\text{m} \times 50\text{ }\mu\text{m} \times 25\text{ }\mu\text{m}$.

Figure 9 shows the positional relation of heated and cooled areas. The location of the center of the cooled area was defined as $(0, Y_c(t))$. The heating with the laser beam was modeled by applying the elliptic Gaussian heat flux, q , calculated by

$$q(Y_c) = \frac{2P'}{\pi\xi_h\eta_h} \exp\left\{-2\left[\frac{x^2}{\xi_h^2} + \frac{(y-Y_c-d)^2}{\eta_h^2}\right]\right\}, \quad (1)$$

where P' is the amount of heat input. $0.64P$ was substituted for P' considering the attenuation of the laser beam by the optical system and the reflection at the glass surface. The cooling with a water jet was modeled by the elliptic Gaussian heat transfer coefficient, α , given by

$$\alpha(Y_c) = \alpha_{\max} \exp\left\{-2\left[\frac{x^2}{\xi_c^2} + \frac{(y-Y_c)^2}{\eta_c^2}\right]\right\}, \quad (2)$$

where α_{\max} is the heat transfer coefficient at the center of the cooled area. In this experiment, the water flow rate

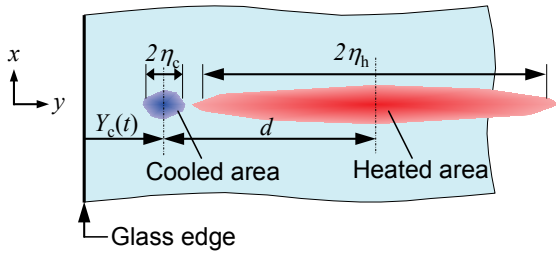


Fig. 9 Positional relation of cooled and heated areas

Table 2 Physical properties of soda lime glass

Density	2520 kg/m ³
Specific heat	800 J/(kg K)
Thermal conductivity	1.03 W/(m K)
Thermal expansion coefficient	8.7×10 ⁻⁶ K ⁻¹
Young's modulus	71.6 GPa
Poisson's ratio	0.23

was 0.8 ml/min, and then, α_{max} was calculated [9] as 1.0×10^5 W/(m² K).

Based on the obtained time variation of the temperature distribution, a thermal stress analysis was conducted. As restraint conditions, x -displacements were set as 0 for nodes on a plane of $x = 0$. y - and z -displacements were set as 0 for nodes on $x = \pm 5$ mm and $z = 700 \mu\text{m}$. Table 2 shows the physical properties used for soda-lime glass [10-12].

3.3 Boundary element analysis

The stress intensity factor, K , was subsequently calculated by BEM in order to conduct a crack propagation analysis. In the laser scribing, a crack propagates due to the tensile stress in the cooled area [3]. Therefore, the modeling region was limited, as the following, to the region sized 6 mm×6 mm×0.7 mm where a crack is likely to propagate. First in cases where we consider the crack propagation phenomenon in the distant area from glass edges, the analysis region was set as $-3 \text{ mm} \leq x \leq 3 \text{ mm}$ and $Y_c - 2 \text{ mm} \leq y \leq Y_c + 4 \text{ mm}$, moving with the movement of the cooled area. Figure 10 shows an example of the mesh geometry used in the BEM analysis. In Fig. 10, a part of a crack with a length of 2 mm is included in the model. Because the crack does not propagate outside of the analysis region, K is not necessary to be obtained there. K changes only a little even when only a part of the whole crack is included in the analysis region. For these reasons, this restriction of the analysis region leads to the reduction of the analysis time, maintaining the accuracy. Next, for the transitional crack propagation phenomenon near the processing start point, the analysis region was fixed as $-3 \text{ mm} \leq x \leq 3 \text{ mm}$ and $0 \leq y \leq 6 \text{ mm}$. When the crack length is less than 6 mm, the entire crack is included in the model and the transitional crack propagation in this region was analyzed. Approximate size of the minimum element was 10 μm , variable according to the crack shape.

With this model the J integral was calculated for each node on the crack front by

$$J = \int_{S_c} \left(W n_i - t_j \frac{\partial u_j}{\partial n_i} \right) dS, \quad (3)$$

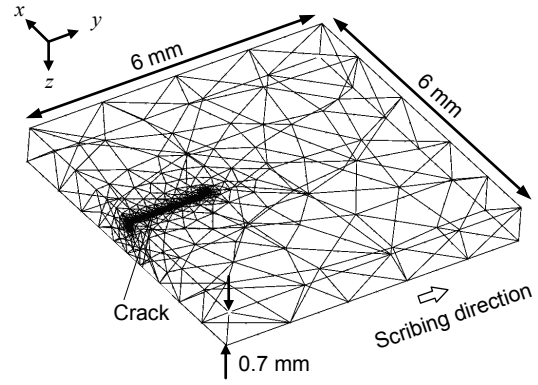


Fig. 10 Example of mesh geometry for BEM analysis in the case where crack tip is at glass center

and K was calculated by

$$K = \sqrt{\frac{E}{1-\nu}} J. \quad (4)$$

In Eqs. (3) and (4), S_c is the circular domain of integration whose center is a node on the crack front, n_i is the normal vector to the crack front, u is the displacement, E is the Young's modulus, and ν is the Poisson's ratio. $W = \sigma_{ij} \varepsilon_{ij} / 2$ and $t_j = \sigma_{ij} n_i$, where σ is the stress and ε is the strain. The sum rule is applied for i and j .

The crack propagation analysis was conducted based on the obtained stress intensity factor. In the laser scribing, in the area ahead of the tensile stress field around the cooled area, there exists a compressive stress field due to the heating with laser beam. This compressive stress field prevents unstable crack propagation. As a result, the crack front locates between the tensile and the compressive stress fields at any time during the processing. In this research, the crack shape at time, t , was obtained by the following way. First an initial crack was set in the tensile stress field and K was calculated under the stress distribution at t . A threshold of the stress intensity factor, K_{th} , was set. When K exceeded K_{th} at some nodes, the crack shape was renewed by moving the nodes in the outward normal direction to the crack front. By this manipulation, the crack propagated only in the region of $K > K_{th}$. The BEM model was remeshed to adapt the new crack shape and then K was recalculated under the same stress distribution. By repeating the K calculation and the crack renewal, the crack propagates to the compressive stress field, resulting in the decrease of K . When K fell below K_{th} at all nodes, the analysis for time t finished. When the transitional crack propagation near the processing start point was considered, the obtained crack shape at one time step was used as the initial crack for the next time step.

Crack growth distance in one step, ΔL , was calculated for each node by

$$\Delta L = C(K - K_{th}). \quad (5)$$

By Eq. (5), ΔL is 0 under $K = K_{th}$ and is larger as K is increased. Here the proportional constant, C , was set as 5×10^{-11} m^{1/2}/Pa. The validities of using Eq. (5) and the value of C are discussed in section 4.1 based on the analysis results.

As explained above, the crack propagation analysis is conducted by comparing K with K_{th} . Because analysis

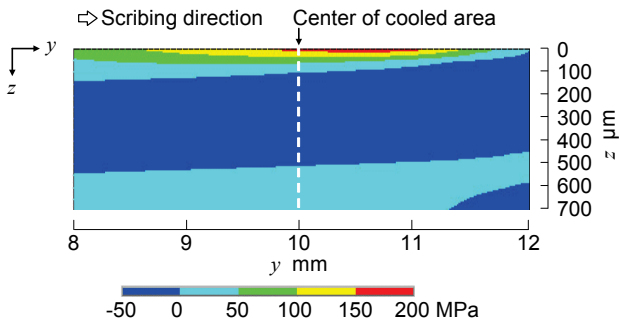


Fig. 11 Stress distribution beneath cooled area in $x = 0$ plane obtained by FEM analysis under $P = 50$ W, $v = 100$ mm/s

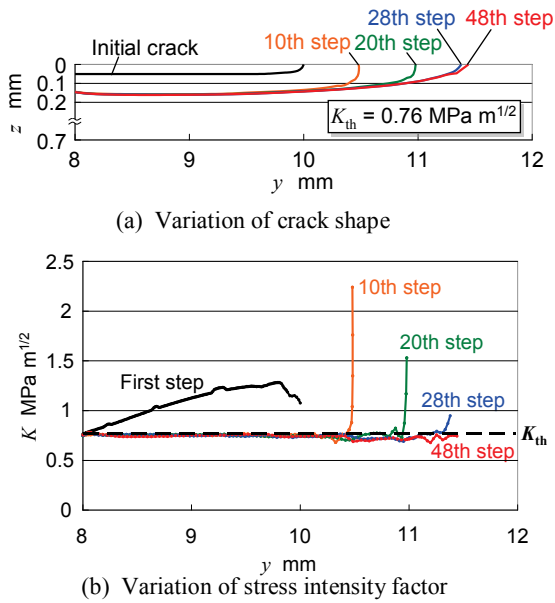


Fig. 12 Variation of analysis results in repeated analysis in the case where $P = 50$ W, $v = 100$ mm/s, $Y_c = 10$ mm

results depend on K_{th} , suitable value of K_{th} should be determined. First in this research, suitable K_{th} was determined focusing on the crack depth at the glass center. Then we considered crack propagation phenomena from the glass edge to the center by applying the obtained K_{th} .

4. Analysis results and consideration

4.1 Determination of suitable value of K_{th}

As an example, one analysis result is explained in the case of $K_{th} = 0.76$ MPa $m^{1/2}$ regarding the condition of $P = 50$ W, $v = 100$ mm/s, and the time step of $Y_c = 10$ mm. At this time step, the center of the cooled area is located at the center of the FEM model. Figure 11 shows the distribution of the normal stress, σ_x , in a plane of $x = 0$ around the cooled area obtained by the FEM analysis. The center of the cooled area ($y = 10$ mm) is shown by a broken line. In the present analysis, the crack shape is obtained by propagating the initial crack set in the tensile stress field. In Fig. 11, σ_x is the maximum at $y = 10.6$ mm, therefore the crack is considered to propagate at least to around this location. Then the y -coordinate of the crack tip was set as 10 mm, less than 10.6 mm. At $y = 10$ mm, σ_x is 0 at the depth of 80

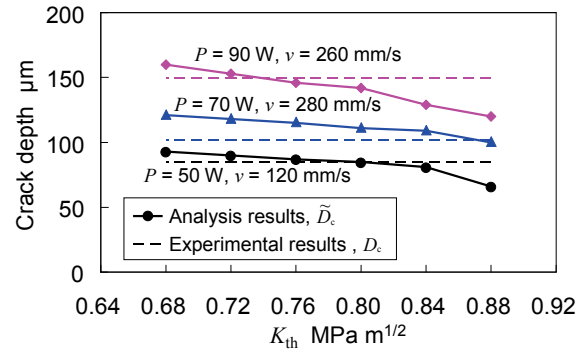


Fig. 13 Crack depth obtained by analysis for a variety of K_{th}

μm . Then the initial crack depth was set as 50 μm , shallower than 80 μm .

Figure 12 shows the variation of the crack shape and K for the analysis progression. The initial crack shape and crack shapes at 10th, 20th, 28th, and 48th steps are shown in Fig. 12 (a). Obtained stress intensity factor, K , for each crack shape is shown in Fig. 12 (b). For the initial crack, K at all nodes exceeded K_{th} . As a result, all parts of the crack front propagated. As the crack propagated K got close to K_{th} . At 10th, 20th, and 28th steps, K exceeded K_{th} only in the region close to the crack tip, and at the 48th step, K fell below K_{th} at all nodes. Final K was almost the same as K_{th} at every node. Therefore the location to which the crack propagates is considered to be obtained by this method.

The obtained crack shape varies depending on K_{th} . Then the suitable value of K_{th} was determined by comparing the crack depth with the measured crack depth, D_c . As shown in Fig. 12 (a), the crack depth in the analysis varies depending on y . In the following, the maximum depth of the crack obtained in the analysis is defined as \tilde{D}_c . Figure 13 shows examples of the variation of \tilde{D}_c under a variety of K_{th} for three processing conditions. The measured crack depth, D_c , in the experiment is also shown by a broken line for each processing condition. In each condition, as K_{th} is decreased, \tilde{D}_c is increased monotonously. K_{th} which minimizes the error of the crack depth, $|\tilde{D}_c - D_c|$, differs depending on the processing condition.

Then we investigated the value of K_{th} which lowers the error averagely in each processing condition by the following way. First the following nine processing conditions were selected from wide region of the process window: (P [W], v [mm/s]) = (50, 80), (50, 120), (50, 160), (70, 160), (70, 220), (70, 280), (90, 260), (90, 320), (90, 380). Next in the nine conditions, \tilde{D}_c was obtained under a variety of K_{th} , and the relative error of \tilde{D}_c for D_c , ε , was calculated for each case by

$$\varepsilon = \frac{|\tilde{D}_c - D_c|}{D_c} \times 100. \quad (6)$$

For each K_{th} , the average value of ε in the nine conditions, $\bar{\varepsilon}$, was calculated. Figure 14 shows the results. The standard deviations of nine ε are shown by error bars and the averages are shown by \bullet . In the case of $K_{th} = 0.76$ MPa $m^{1/2}$, $\bar{\varepsilon}$ was 5.5 %, which was the minimal and minimum value. Therefore, for the selected nine conditions, 0.76 MPa $m^{1/2}$ is suitable for K_{th} .

Next, in the cases of $P = 60, 80$ W, \tilde{D}_c was obtained under $K_{th} = 0.76$ MPa m^{1/2} and was compared with D_c . Note that the conditions of $P = 60, 80$ W were not used to determine K_{th} . Figure 15 shows the results. Regarding the nineteen conditions shown in Fig. 15, the average of ε was 6.6 %. Also in the cases of $P = 60, 80$ W, \tilde{D}_c well agreed with D_c by setting K_{th} as 0.76 MPa m^{1/2}. From these results, it is found that the same value is applicable as suitable K_{th} even when P and v are varied. Therefore, by investigating suitable K_{th} with a part of conditions, the crack depth under other conditions with different P and v can be estimated.

In this analysis, if the crack growth distance in one step, ΔL , is too large, there is a possibility that the crack propagates further than the location where $K = K_{th}$, resulting in lower K than K_{th} . From the result that K at the final step was nearly equal to K_{th} at all nodes as shown in Fig. 12 (b), it can be said that ΔL set by Eq. (5) was low enough for the proper results, and that the value of C in Eq. (5) is proper. Besides by making ΔL larger as K is increased by Eq. (5), relatively smooth crack fronts could be obtained at each step as shown in Fig. 12 (a).

4.2 Crack propagation in the area around glass center

We considered the crack propagation phenomena around the glass center by applying the obtained K_{th} . As shown in Fig. 4, a crack of constant depth is observed in the glass center. Figure 16 shows crack shapes obtained in the analysis for three time steps when the center of the cooled area is around the glass center ($Y_c = 9, 10, 11$ mm). The crack shapes were almost the same among three time steps, and the crack tip moved in the y -direction by the same distance as the movement distance of the cooled area. That is to say, the crack propagated quasi-steadily around the glass center. From these results, it is concluded that quasi-steady crack propagation results in the formation of one crack of constant depth as shown in Fig. 4. And this is the reason why the crack depth can be estimated from the static stress distribution at certain time as shown in section 4.1.

4.3 Crack propagation around processing start

Next, the transitional crack propagation phenomenon near the processing start point was considered. The value of K_{th} obtained in section 4.1 (0.76 MPa m^{1/2}) was applied here. Figure 17 shows the variation of the normal stress (σ_x) distribution in a plane of $x = 0$ obtained by the FEM analysis. The location of heated and cooled areas for each time step is schematically shown in the left of the stress distribution figures. In Fig. 17, during the period of -20 mm $\leq Y_c \leq -2$ mm, the glass edge is heated by the laser beam. In this period, the compressive stress is generated in the vicinity of the upper surface while the tensile stress is generated inside the glass. In the subsequent period of $Y_c \geq -2$ mm, the cooled area passes above the substrate. In this period, the tensile stress is generated not only inside but also in the vicinity of the upper surface. The tensile stress field on the upper surface moves in the y -direction with time, while the inside tensile stress is lowered without moving. The variation of the crack shape was analyzed for such transitional variation of the stress distribution.

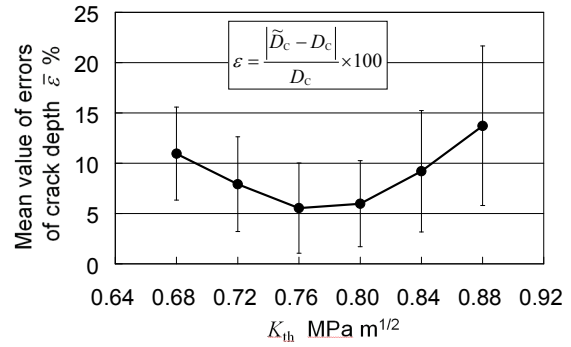


Fig. 14 Mean value of errors of analyzed crack depth for measured crack depth under a variety of K_{th}

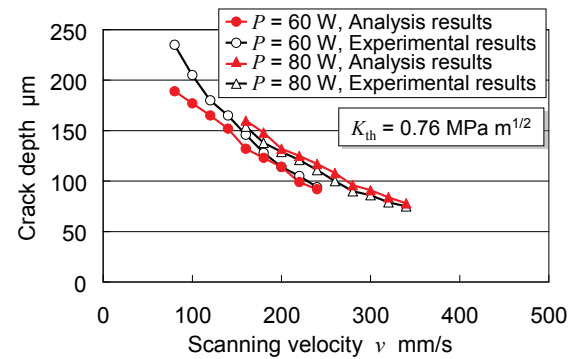


Fig. 15 Comparison of measured and analyzed crack depth in case of $K_{th} = 0.76$ MPa m^{1/2}

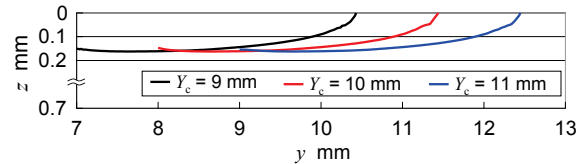


Fig. 16 Comparison of crack shapes obtained for three different time steps where $Y_c = 9, 10, 11$ mm

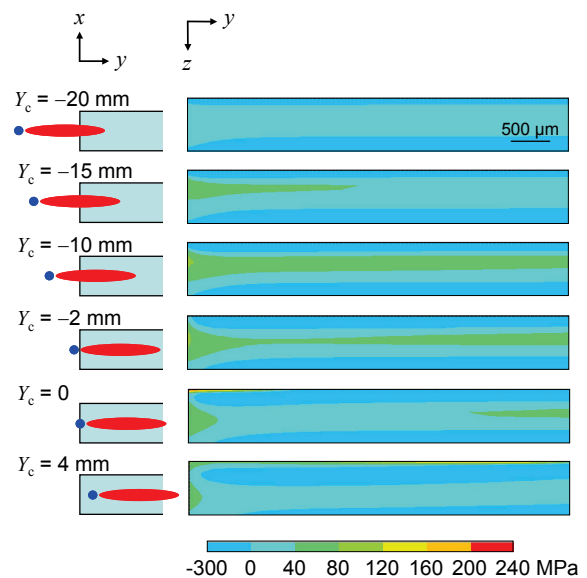


Fig. 17 Variation of stress distribution near processing start under $P = 90$ W, $v = 380$ mm/s

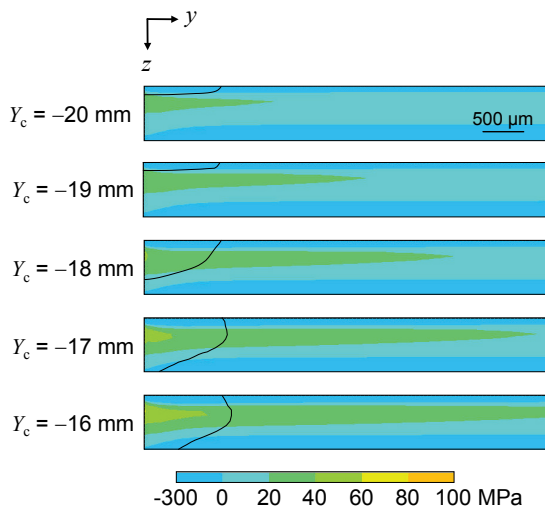


Fig. 18 Variation of analysis results of crack shape near processing start under $P = 90$ W, $v = 380$ mm/s during period when glass edge is heated

4.3.1 Formation of through crack

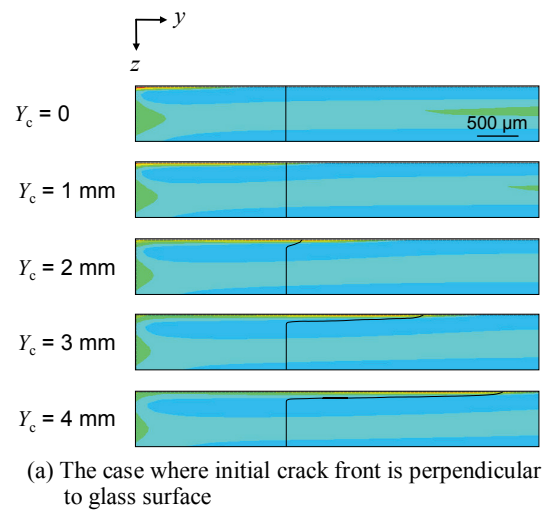
We firstly investigated how the initial crack propagates in the period when the glass edge is heated. The initial crack shape in the analysis was set to be the same as the measured crack in the experiment shown in Fig. 3. Figure 18 shows the variation of the crack shape in the condition of $P = 90$ W and $v = 380$ mm/s. Solid lines in Fig. 18 indicate the crack fronts at each time step. At the time step of $Y_c = -20$ mm, K fell below K_{th} at all nodes, resulting in no crack propagation. At the time step of $Y_c = -19$ mm, the crack started to propagate and propagated more in the z -direction than in the y -direction. At the time step of $Y_c = -17$ mm, the crack reached the bottom surface to become a through crack. After that the through crack propagated in the y -direction.

The tensile stress is generated only inside the glass at every time step in Fig. 18, and the crack propagated with the increase of the tensile stress. From these results, it is concluded that the through crack is formed at the glass edge due to the inside tensile stress generated while the glass edge is heated.

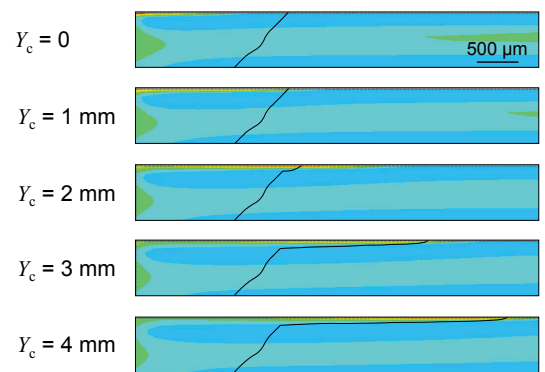
4.3.2 Transition from through crack to surface crack

Subsequently we considered the phenomenon that a through crack transitions into a surface crack at a certain location. As mentioned above, an initial crack changes into a through crack due to the inside tensile stress in the period when the glass edge is heated. Subsequently, after the cooled area reaches the glass edge, the tensile stress is generated also in the vicinity of the upper surface. Here we investigated how the through crack propagates in the cooling period, setting a through crack as an initial crack.

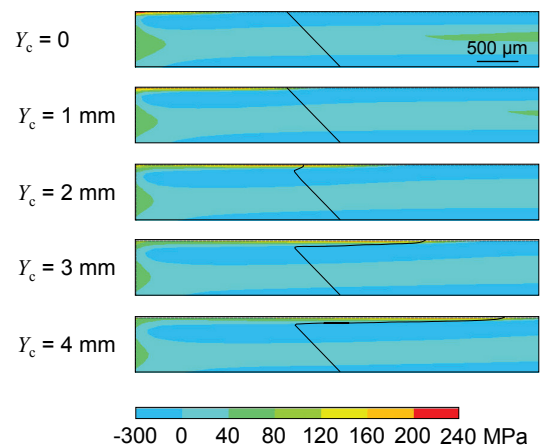
First the initial through crack was set, having a perpendicular front to the glass surface with length of 2 mm in the y -direction. Figure 19 (a) shows the crack propagation process. At the time step of $Y_c = 0$, 1 mm, the crack did not grow. At the time step of $Y_c = 2$ mm, a part of the crack front propagated near the laser beam irradiated surface. After that the crack propagated only in the vicinity of the upper surface with the movement of the tensile stress field



(a) The case where initial crack front is perpendicular to glass surface



(b) The case where initial crack front crosses glass surface at 45 degrees and crack precedes at top surface



(c) The case where initial crack front cross glass surface at 45 degrees and crack precedes at bottom surface

Fig. 19 Variation of analysis results of crack shape near processing start under $P = 90$ W, $v = 380$ mm/s during period when glass edge is cooled

in the y -direction. As a result, a surface crack was formed to rearward of the through crack. Although the inside tensile stress field exists also in the cooling period, the magnitude is lower than that in the heating period. Besides the further area from the glass edge has lower inside tensile stress. These are considered to be the reason why the crack

propagates only in the vicinity of the upper surface during the cooling period.

As a through crack formed in the heating period, other cases can be considered where the crack front does not cross the glass surface at right angles. Then we also analyzed the additional two cases where the through crack front crosses the glass surface at 45 degrees. Figure 19 (b) and (c) show contrastive cases where the crack precedes in the upper and bottom side respectively. In both cases, after the time step of $Y_c = 1$ mm, the crack propagated only in the vicinity of the upper surface with the movement of the cooled area. As a result, a surface crack was formed. One difference is that, in (b), the inside part of the through crack propagated at the time step of $Y_c = 0$. The reason is considered to be because the crack front was close to the glass edge and was located where the tensile stress was high enough to grow the crack.

In either case, a surface crack was formed from a through crack during the cooling period regardless of the through crack shape. Besides the propagation of the surface crack under the cooled area was not influenced by the through crack shape. From these results, it is concluded that a surface crack is formed rearward of the through crack due to the tensile stress in the vicinity of the laser beam irradiated surface which is generated in the cooling period.

5. Conclusions

First in this research, we experimentally investigated how the crack propagates from the processing start to the glass center. It was found that a through crack was formed in the area within some millimeters from the processing start and a surface crack of constant depth was formed in the following region. In order to clarify the mechanism of such transitional crack propagation, we conducted a three-dimensional crack propagation analysis by combining FEM and BEM. The obtained conclusions are as follows:

1. In the period when the glass edge is heated, the tensile stress is generated inside the glass near the glass edge. An initial crack propagates in the thickness direction due to this tensile stress, to become a through crack.
2. In the subsequent period when the glass edge is cooled down, the tensile stress is generated also in the vicinity of the laser beam irradiated surface. The through crack propagates only in the vicinity of the glass surface due to this tensile stress. In this period the crack propagates quasi-steadily, to form a surface crack of constant depth.
3. Regarding the quasi-steady crack propagation, the crack depth obtained by the analysis agrees well with the measurement result by applying a suitable threshold of the stress intensity factor, K_{th} . Even when the laser power, P , and the scanning velocity, v , are varied, the same value can be applied for suitable K_{th} .
4. Therefore, by investigating suitable K_{th} with a part of processing conditions, the crack depth under other conditions with different P and v can be estimated.

References

- [1] S.C. Wang, L.Y. Yeh, C.C. Lin, M.S. Chen, and F.Y. Gan: Proc. of the 14th Int. Display Workshops, Sapporo, (2007), p.513.
- [2] V.S. Kondratenko: PTC WO 93/20015 (1993)
- [3] K. Yamamoto, N. Hasaka, H. Morita, and E. Ohmura: J. Laser Appl., 20, (2008), 193.
- [4] Y. Miyake: J. Jpn. Soc. Abra. Tech., 45, (2001), 342.
- [5] K. Yahata, K. Yamamoto, and E. Ohmura: J. Laser Micro/Nanoengineering, 5, (2010), 109.
- [6] K. Yamamoto, N. Hasaka, H. Morita, and E. Ohmura: Prec. Eng., 32, (2008), 301.
- [7] A. Portela: "Dual boundary element analysis of crack growth", (Computational Mechanics Publications, 1993)
- [8] K. Yahata, E. Ohmura, S. Shimizu, M. Murakami: Proc. of 6th Int. Conf. on LEM21, Saitama, (2011), p.3374.
- [9] A. Yamamoto: J. Jpn Soc. Prec. Eng., 26, (1960), 461.
- [10] The Japan Society of Mechanical Engineers ed.: "JSME Data Handbook: Heat Transfer, 4th Ed.", (The Japan Society of Mechanical Engineers, 1986)
- [11] E.B. Shand: "Glass Engineering Handbook, 2nd ed.", (McGraw-Hill, 1958)
- [12] M. Yamame, I. Yasui, M. Wada, Y. Kokubu, R. Terai, K. Kondo, and S. Ogawa: "Glass Engineering Handbook", (Asakura Shoten, 1999)

(Received: October 23, 2012, Accepted: January 30, 2013)